Astron. Astrophys. 336, 980–985 (1998)

ASTRONOMY
AND
ASTROPHYSICS

How thin B[e] supergiant disks can be?

Ph. Stee

Observatoire de la Côte d'Azur, Département FRESNEL, CNRS UMR 6528, 2130, route de l'Observatoire, Caussols, F-06460 St. Vallier de Thiey, France

Received 29 January 1998 / Accepted 4 June 1998

Abstract. We investigate the shape of the envelope around B[e] supergiant stars using a model developed by Stee & Araùjo (1994) for Be stars. We obtain mass loss rates $\dot{M}$ between $5.5 \cdot 10^{-7}$ and $6.2 \cdot 10^{-6}$ $M_{\odot}yr^{-1}$ depending on mass flux variation from polar to equatorial regions. We find that winds from B[e] stars can be so dense that they become optically thick in the continuum, masking the photosphere of the central star. For mass loss rates larger than $10^{-5}M_{\odot}yr^{-1}$ it is not possible to see the stellar photosphere even for pole-on B[e] stars. Using a two-component wind model driven by optically thin lines in the equatorial regions and optically thick lines in the polar regions, we obtain a relation between the geometry of the envelope and the total mass loss. We also put limits on the inclination angle (i) beyond which the stellar photosphere is masked. Finally, this study seems to discard "wind-compressed disks" (WCD) models as a possible senario for B[e] supergiant envelopes.

Key words: circumstellar matter – stars: emission-line, Be – stars: mass-loss – stars: supergiants

1. Introduction

The group of hot supergiants B[e] stars shows strong IR excess due to free-free and free-bound emission which also requires the formation and emission from dust (Zickgraf 1990). These stars exhibit narrow forbidden and permitted emission lines of low excitation species at visible wavelengths and broad absorption lines of highly ionized ions in the UV. They show evidence for axially symmetric winds (Zickgraf et al. 1989, 1992) and their mass loss rates can attain 10^{-5} $M_{\odot}yr^{-1}$ to 10^{-4} $M_{\odot}yr^{-1}$ (Zickgraf et al. 1992). Most of the time it is very difficult to assign them a given spectral type since their dense and massive expanding winds mask the photospheric lines (Carlson & Henize, 1979). In this paper we study the effect of envelope geometry and thickness on the continuum emission by using a radiative wind model developed by Stee & Araùjo (1994) for "normal" Be stars and modified by Stee et al. (1995, hereafter Paper I). The stellar parameters used in this model, taken from Araùjo et al. (1994), are given in Table 1. In Sect. 2 the basic assumptions and results of the model are outlined. Sect. 3 presents the different geometrical shapes of the envelope and the corresponding continuum fluxes for different inclination angles. In Sect. 4 the effect of the envelope opacity on the stellar continuum is investigated. The main results of our study are summarized and discussed in the last section.

Send offprint requests to: stee@obs-nice.fr

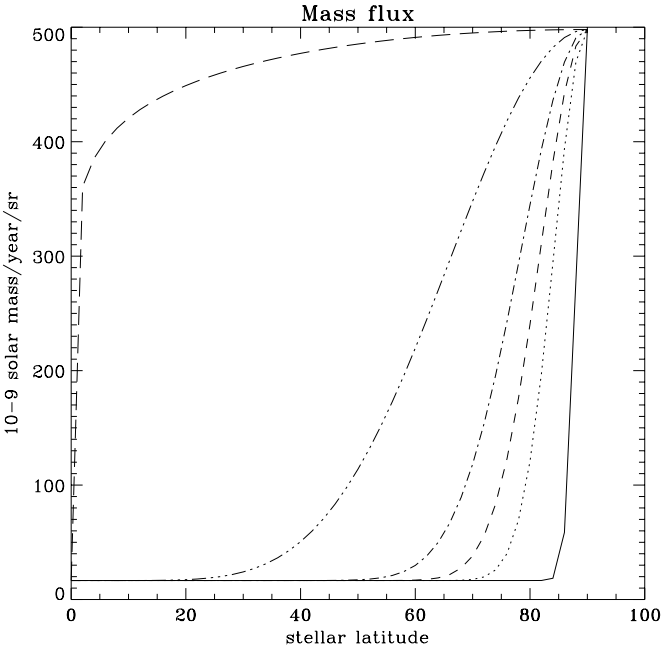

Fig. 1. Variation of the mass flux in unit of 10^{-9} $M_{\odot}$ yr^{-1} sr^{-1} as a function of the stellar latitude and $m1$ parameter. Solid line: $m1$=1000, dotted: $m1$=100, dashed: $m1$=50, dash dot: $m1$=25, dash dot dot dot: $m1$= 6, long dashes: $m1$=0.1

2. A model for B[e] stars

2.1. Main hypothesis

The basic equations of our model are described in detail in Paper I. This model is steady-state and axi-symmetric with respect to the rotational axis. No meridian circulation is allowed. The polar wind is represented by a CAK-type stellar wind model with a mass flux of $1.6 \cdot 10^{-8}$ $M_{\odot}yr^{-1}sr^{-1}$ and a terminal wind velocity of V_{∞}=600 km s^{-1} whereas in the equatorial regions,

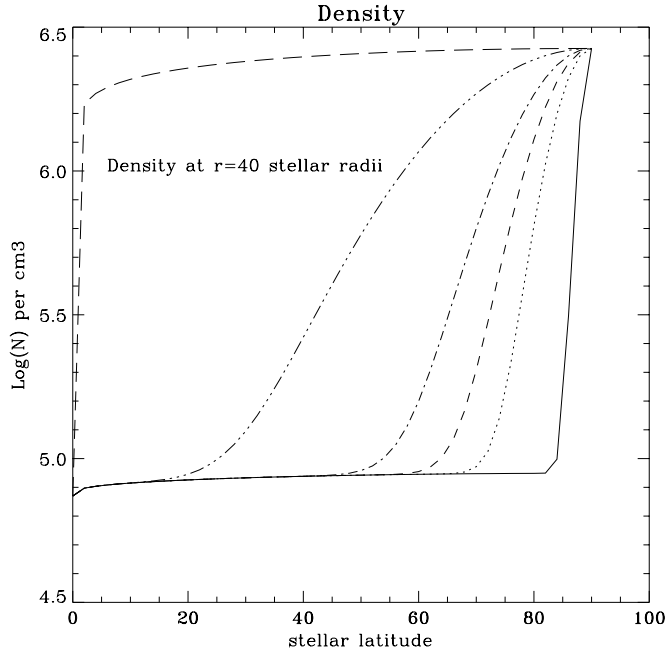

Fig. 2. Variation of the envelope density at 40 stellar radii as a function of the stellar latitude. Solid line: $m1$=1000, dotted: $m1$=100, dashed: $m1$=50, dash dot: $m1$=25, dash dot dot dot: $m1$= 6, long dashes: $m1$=0.1

Table 1. Parameters used for a typical B[e] supergiant (from Araùjo et al. 1994)

Parameters	
Spectral type	B1Ie
Effective temperature	20000 K
Mass	30 $M_\odot$
Radius	75 $R_\odot$
Luminosity	10^6 $L_\odot$
Polar terminal velocity	600 km s^{-1}
Polar mass flux	$1.6 \cdot 10^{-8}$ $M_\odot$ yr^{-1} sr^{-1}
Equatorial terminal velocity	500 km s^{-1}
Equatorial mass flux	$5.0 \cdot 10^{-7}$ $M_\odot$ yr^{-1} sr^{-1}
Rotational velocity	135 km s^{-1}

the mass flux is $5.0 \cdot 10^{-7}$ $M_\odot yr^{-1} sr^{-1}$ and V_∞=500 km s^{-1}. This leads to a ratio between the equatorial and polar mass flux (C1) of ∼30 (the same value used for the modelling of γ Cas in Paper I). The other basic stellar parameters are summarized in Table 1.

We used the following expression for the variation of the mass flux as a function of the stellar latitude:

$$\Phi(\theta) = \Phi_{pole} + [(\Phi_{eq} - \Phi_{pole}) \sin^{m1}(\theta)], \quad (1)$$

where $m1$ is a free parameter which describes the variation of the mass flux from the pole to the equator (see Fig. 1).

Following Paper I, the density distribution in the envelope is given by:

$$\rho(r,\theta) = \frac{\Phi(\theta)}{(\frac{r}{R})^2 v_r(r,\theta)}. \quad (2)$$

Table 2. Mass loss rate as a function of the m1 parameter

$m1$	Mass loss in 10^{-6} $M_\odot yr^{-1}$
1000	0.55
100	1.06
50	1.37
25	1.78
6	3.08
0.1	6.18

with $v_r(r,\theta) = \frac{\Phi_{pole}[1+(C1-1)\sin^{m1}(\theta)]}{\rho_0} +$
$+\big(V_\infty(pole) + [V_\infty(eq) - V_\infty(pole)]\sin^{m2}(\theta) -$

$$- \frac{\Phi_{pole}[1 + (C1-1)\sin^{m1}(\theta)]}{\rho_0}\big)(1 - \frac{R}{r})^\beta. \quad (3)$$

where R is the stellar radius and $m2$=0.3. Note that Eq. (3) is a β-velocity law with β = 0.86 (the same value used in Paper I). This last value agrees with β = 0.77 obtained by Miroshnichenko (1996) by fitting Balmer line profiles from the supergiant MWC 314 which also presents a stellar wind with a quite low terminal velocity (500 km s^{-1}).

The value of $m2$, which is a free parameter characterizing the variation of the terminal velocity from pole to equator, is not as critical as for γ Cas. Since the terminal velocities are comparable in this case (respectively 600 and 500 km s^{-1} at the pole and at the equator) and the continuum emission is not sensitive to the kinematics of the disk, we have taken $m2$=0.3, as in Paper I. Moreover, we have tested different values for $m2$ without noticeable change in the continuum energy distribution.

2.2. Different envelope geometries

Following Eq.(1) and Eq. (2) the m1 parameter produces different variations of the envelope density as a function of stellar latitude (Fig. 2). In this study we have computed different models for 6 values of $m1$ which are respectively 1000, 100, 50, 25, 6 and 0.1 producing different envelope shapes starting from a very flat disk (top left in Fig. 3) and a more or less ellipsoidal envelope (bottom right in Fig. 3). Note that in the case of $m1$=1000, the envelope resembles a "pan-cake" with a central bulge due to the constant hydrogen density between 0 and 85 degree. After 85 degree the hydrogen density increases by a factor of 35 and forms a very flat and dense disk. From $m1$=1000 to $m1$=0.1, the density increases closer to the polar latitudes and thus, this "bulge" is less and less visible.

For different values of $m1$ we have computed the corresponding mass loss rates, summarized in Table 2, ranging from $5.5 \cdot 10^{-7}$ to $6.2 \cdot 10^{-6}$ $M_\odot yr^{-1}$. These mass loss rates are in the range of those obtained by Zickgraf et al. (1996), i.e. $5 \cdot 10^{-7}$ $M_\odot yr^{-1}$ or $6 \cdot 10^{-7}$ $M_\odot yr^{-1}$ for the B[e] stars Hen S22 and R82 in the Large Magellanic Cloud.

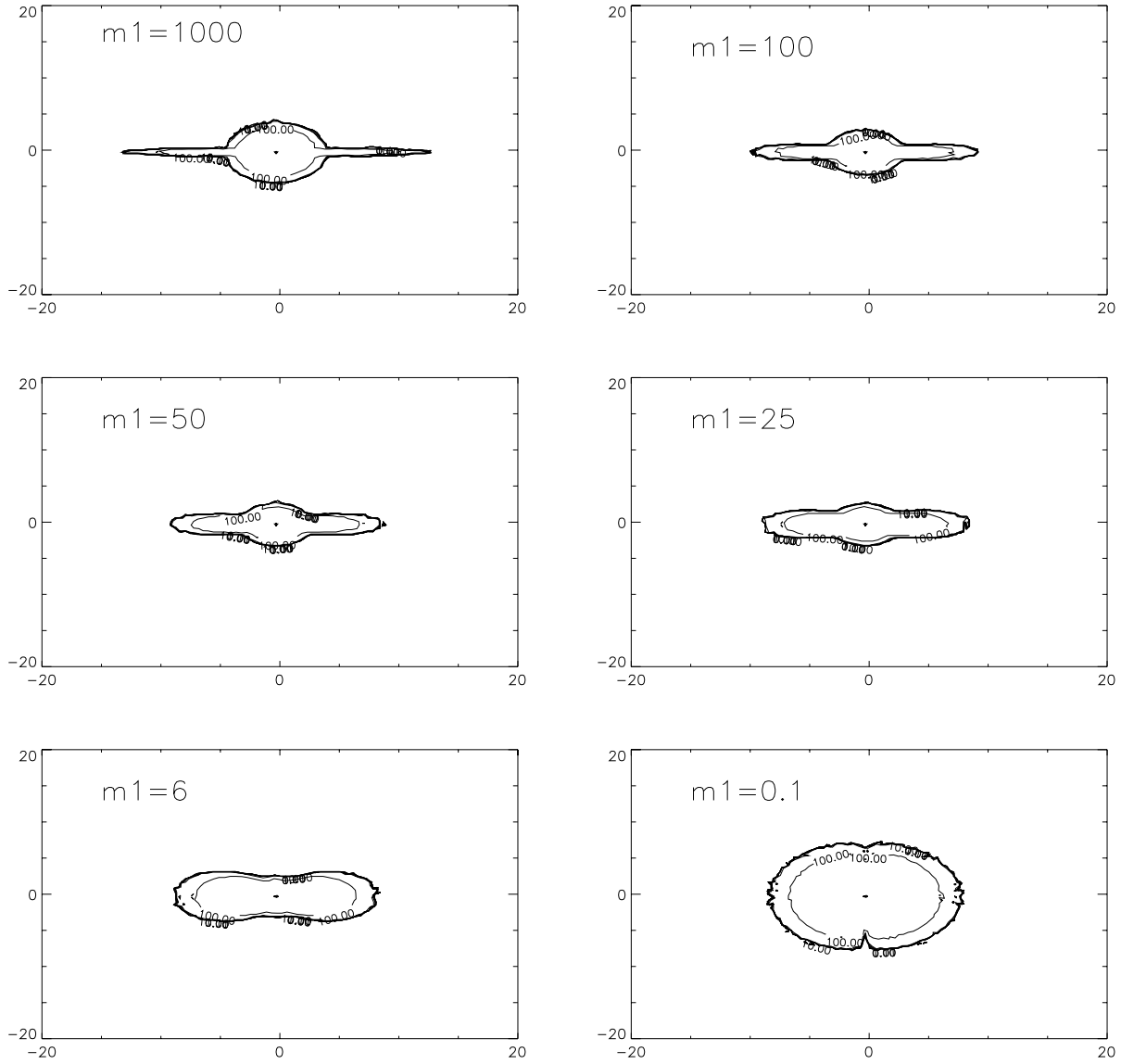

Fig. 3. Meridional isodensity curves for the envelope. From upper left to lower right the value of m1 is respectively 1000, 100, 50, 25, 6 and 0.1. The contours levels are 100, 50, 10, 5, 1, 0.5, 0.05, 0.01, axes are in units of stellar radius.

3. The continuum source function

In order to study the continuum emission which originates from different envelope geometries we have computed the continuum source function of a pure hydrogen gas. We have taken into account free-free and free-bound emission, and for absorption coefficients of free-free and scattering mechanisms. The free-free emission coefficient is given by:

$$\eta_{f-f} = 5.441\,10^{-39} g_{f-f} {n_e}^2 T^{-1/2} \mathrm{e}^{\frac{-h\nu}{kT}} \quad (4)$$

the free-bound emission coefficient for $\nu \gtrsim \nu_{ci}$ (ν_{ci} is the i^{th} series limit frequency) is

$$\eta_{f-b} = \sum_{i=1}^{6} 2.14\,10^{-32} g_{f-f} {n_e}^2 i^{-3} T^{-3/2} \mathrm{e}^{\frac{h(\nu_{ci}-\nu)}{kT}} \quad (5)$$

the free-free absorption coefficient is:

$$\kappa_{f-f} = 3.69\,10^{8} g_{f-f} {n_e}^2 T^{-1/2} \nu^{-3} (1 - \mathrm{e}^{\frac{-h\nu}{kT}}) \quad (6)$$

and the scattering coefficient is $n_e\sigma$.

The gaunt factor g_{f-f} was taken from Pottasch (1984):

$$g_{f-f} = \frac{3^{1/2}}{\pi} ln(\frac{4.95\,10^{-2} T^{3/2}}{\nu z}) \quad (7)$$

where the frequency ν is given in Ghz (10^9 Hz) and z is the ionic charge. The absorption by the envelope of the stellar radiation (with T_{eff}= 20000 K), is also taken into account. The envelope temperature distribution is given by:

$$T(r) = T_{eff} \Big(\frac{R}{r}\Big)^{0.5}. \quad (8)$$

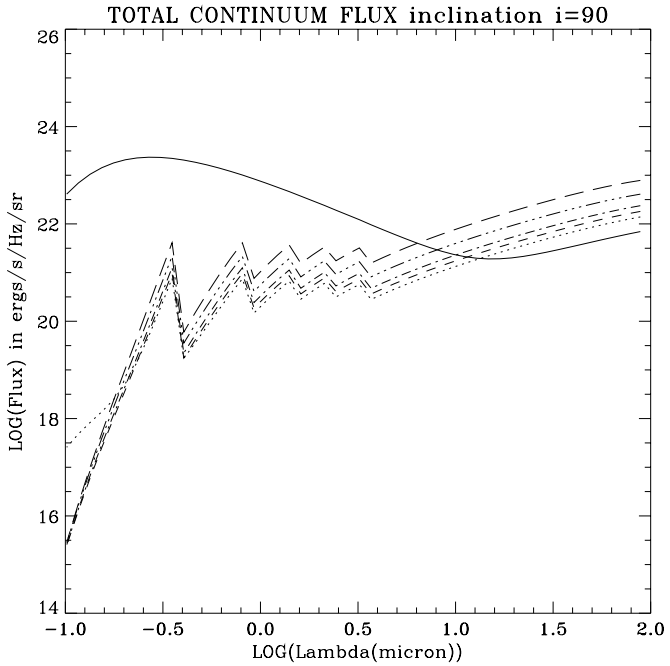

Fig. 4. Total continuum emission (star + envelope) in ergs s^{-1} Hz^{-1} sr^{-1} seen equator-on. Solid line: $m1$=1000, dotted: $m1$=100, dashed: $m1$=50, dash dot: $m1$=25, dash dot dot dot: $m1$= 6, long dashes: $m1$=0.1

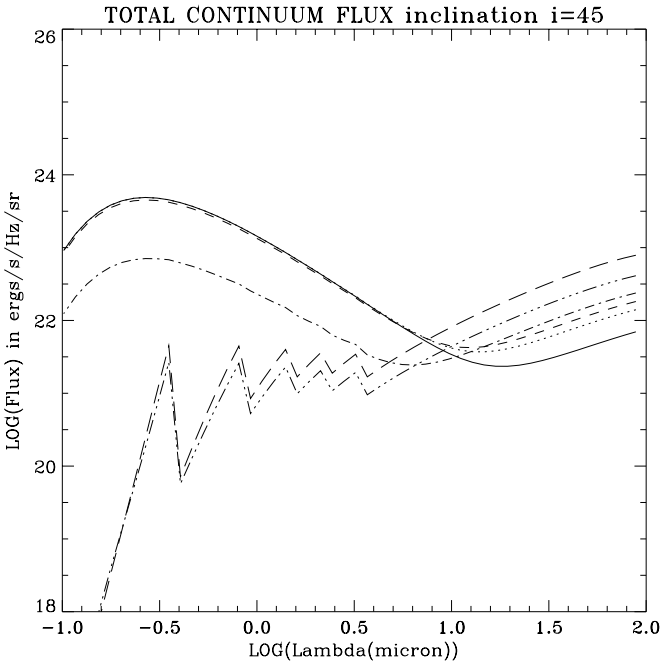

Fig. 5. Total continuum emission (star + envelope) in ergs s^{-1} Hz^{-1} sr^{-1} for $i = 45°$. Solid line: $m1$=1000, dotted: $m1$=100, dashed: $m1$=50, dash dot: $m1$=25, dash dot dot dot: $m1$= 6, long dashes: $m1$=0.1

The computation was done for 3 different inclination angles: equator-on ($i = 90°$), intermediate ($i = 45°$) and pole-on ($i = 0°$).

4. Results

The continuum emissions are plotted in Figs. 4, 5 and 6. From Fig. 4 (equator-on case) it can be shown that only a very flat envelope ($m1$=1000) produces a smooth energy distribution from 0.1 to 10 μm without Balmer-series jump. It means that for $m1$=1000 the total continuum emission is dominated by the stellar emission up to 10 μm. After 10 μm the stellar emission is absorbed and reemitted by the envelope which is increasing the total continuum emission at larger wavelengths.

For all the other models the total flux is dominated by the envelope emission, except for $m1$=100, between 0.1 and 0.2 μm where the stellar contribution is higher than the envelope one. It is more obvious in Fig. 7, where we can see that up to 12 μm the continuum flux is dominated by the stellar contribution.

For an intermediate inclination, i.e. ($i = 45°$), the situation is less pronounced and for $m1$=1000, 100, 50 and 25 the stellar flux dominate the spectrum up to 8 μm (see Fig. 5).

For the pole-one case (see Fig. 6), the stellar continuum dominates the spectrum up to 16, 12, 11, 10, 9 and 8 μm respectively for $m1$= 1000, 100, 50, 25, 6 and 0.1.
In fact two effects occur:

- The stellar continuum emission is more absorbed when the observer goes from the polar regions to the equatorial one due to an increase in the optical depth.

- The continuum flux emitted from the envelope increases in correlation with the envelope size, i.e. for smaller values of $m1$.

Both effects tend to decrease the ratio stellar/envelope continua.

5. Discussion

5.1. Do we see photospheric features on B[e] stars?

In Fig. 8 we have plotted the envelope shape ($m1$ parameter) as a function of mass loss rate in units of 10^{-6} $M_{\odot}yr^{-1}$. As already mentioned, the mass loss increases as the envelope becomes more and more ellipsoidal (lower m1). We have also plotted 3 horizontal lines for different inclination angles (i=0, 45 and 90°). The region above each line is a region from which it is possible to see the stellar photosphere. For i=**0 ° (pole-on) it is possible to see photospheric features for all the models**, for i=45°, only models with $m1$ larger than 25 allow to observe photospheric features wherease **for equator-on stars the envelope must be very flattened**, i.e. $m1$ larger than 100.

5.2. Effect of the terminal velocity of the wind

We have studied the effect of changing the terminal velocity in the polar direction from V_{∞}=600 km s^{-1} up to V_{∞}=2000 km s^{-1} without noticeable change in our results. In fact, a more interesting quantity is the polar/equatorial terminal velocity ratio which can be of the order of 10 (see Gummersbach et al. 1995). This leads to a two-component stellar wind model which was

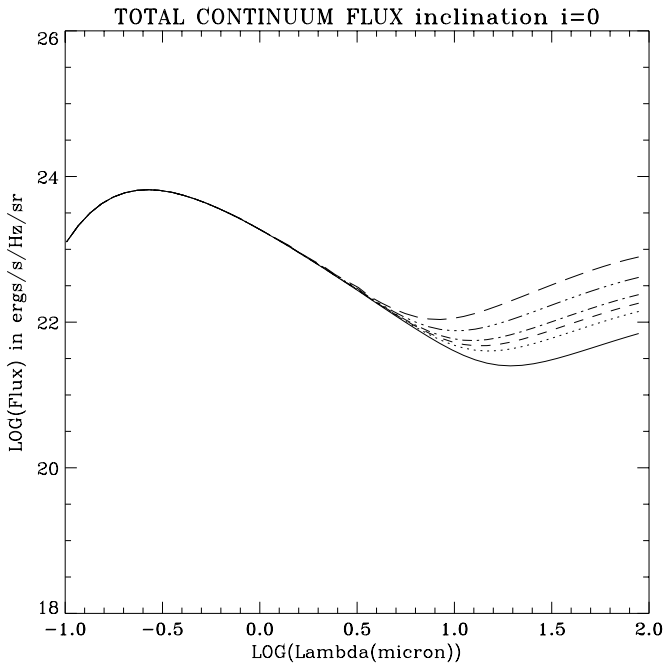

Fig. 6. Total continuum emission (star + envelope) in ergs s^{-1} Hz^{-1} sr^{-1} seen pole-on. Solid line: $m1$=1000, dotted: $m1$=100, dashed: $m1$=50, dash dot: $m1$=25, dash dot dot dot: $m1$= 6, long dashes: $m1$=0.1

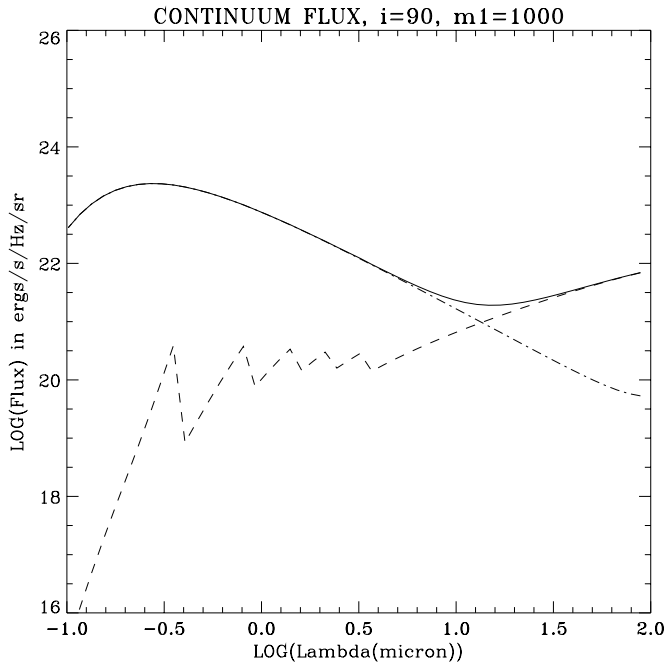

Fig. 7. Continuum emission in ergs s^{-1} Hz^{-1} sr^{-1} seen equator-on for $m1$=1000. Solid line: total emission, long dashed: envelope emission, dash dot: stellar emission

a scheme already found in Paper I for γ Cas. Moreover Araùjo (1995) has shown that equatorial regions driven mainly by optically thin lines and polar regions driven by optically thick lines can lead to a polar/equatorial terminal velocity ratio of 10. This

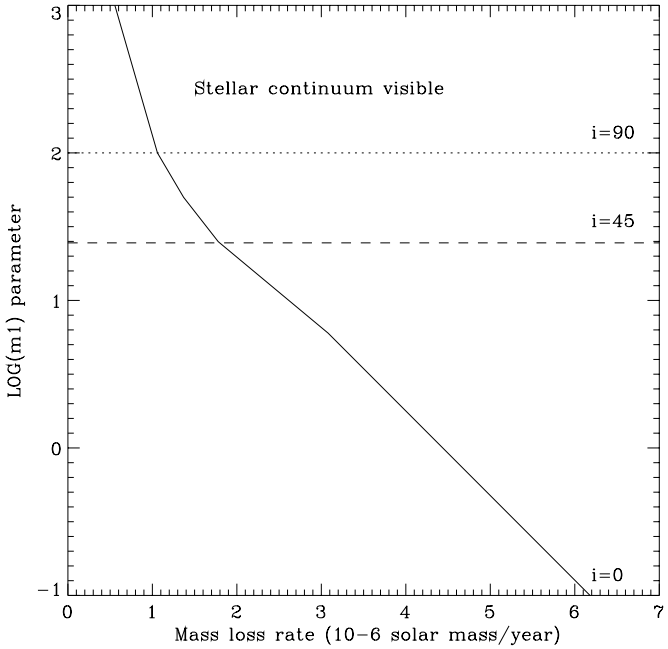

Fig. 8. Envelope shape ($m1$ parameter) as a function of the mass loss rate in unit of 10^{-6} $M_{\odot}yr^{-1}$. We have plotted 3 horizontal lines for different inclination angles (i=0, 45 and 90°) from which it is possible to see the stellar photosphere (region above each line). Note that for $i = 0°$ the horizontal line is superposed with the absissa axe

distinction between a wind driven by optically thin/thick lines can also be a basic property for B[e] stars.

In order to study this effect we have computed another complete set of models with an equatorial terminal velocity of V_{∞}=100 km s^{-1} and a polar terminal velocity of V_{∞}=1000 km s^{-1}. This produces an increase in the continuum emission from the equatorial regions and the effect of masking photospheric features appears for inclination angles smaller than for the previous model, i.e. in Fig. 8 you can replace the horizontal lines with inclination angles of 45 and 90° by inclination angles of 35 and 80°. Nevertheless, even for the very flattened model ($m1$=1000), the stellar continuum was not completely absorbed and it was not possible to hide photospheric features for the very thin model.

5.3. Effect of the mass flux

We have also investigated the effect of increasing the polar mass flux and thus the total mass loss rate. We have started from a total loss rate of 10^{-6} $M_{\odot}yr^{-1}$ and increase the mass loss rate at each step by a factor of 2. **For mass loss rates larger than 10^{-5} $M_{\odot}yr^{-1}$ it is not possible to see the stellar photosphere even for pole-on B[e] stars**. All the stellar continuum emission is absorbed and reemitted by the envelope, masking completely photospheric features. It means that absorption features observed in these objects are interstellar or circumstellar absorptions.

6. Conclusion

Absorption of the stellar continuum and reemission by the envelope appears to be a crucial phenomenon among B[e] supergiant stars which show no clear evidence for photospheric lines. In addition strong emission lines can also mask underlying photospheric absorption lines. Nevertheless all photospheric lines cannot be filled only by emission lines and the stellar continuum absorption and reemission by the envelope must be take into account for B[e] stars with stellar winds larger than 10^{-5} $M_{\odot}yr^{-1}$. Finally it appears that very flat disks as predicted by "wind-compressed disk" (WCD) models proposed by Bjorkman & Cassinelli (1993) have serious difficulties to mask the photosphere whereas no photospheric feature are usually seen in the optical spectrum (Pacheco 1998). For instance, recent observations of the high luminosity peculiar Be star MWC 314 by Miroshnichenko (1996), with a mass loss rate of $3 \cdot 10^{-5}$ $M_{\odot}yr^{-1}$ show no evidence of photospheric lines and spectral features. In conclusion the results of this present study seems to discard the WCD model as a possible senario for B[e] supergiant envelopes, keeping in mind that, from a self-consistent dynamical simulation, Owocki et al. 1996 also showed that non radial line forces inhibit in fact the formation of a WCD.

We intend to present in a near future an improved model with **gas and dust** in order to directly compare computed spectral energy distribution with observational data of B[e] stars.

Acknowledgements. I am indebted to H.J.C.L.M. Lamers for encouraging me for the present work. This study was also stimulated by useful discussions and suggestions from F. Vakili. I am also grateful to J. Pacheco for his constructive comments and suggestions. Finally I thank the referee, O. Stahl for comments that helped to improve the presentation of this paper.

References

Araùjo, F.X., Freitas Pacheco, J.A., Petrini, D. 1994, MNRAS, 267, 501
Bjorkman, J. E., & Cassinelli, J. P. 1993, ApJ, 409, 429
Carlson, E.D., Henize, K.G. 1979, Vistas Astron. 23, 213
Gummersbach C.A., Zickgraf F.-J. and Wolf B. 1995, A&A, 302, 409
Mc Gregor, P.J., Hyland., A.R., Hillier, D.J. 1988, ApJ 324, 1071
Miroshnichenko A. S. 1996, A&A, 312, 941
Owocki, S.P., Cranmer, S.R. and Gayley, K.G. 1996, ApJ 472, L115
Pacheco, J.A. 1998, Workshop on B[e] stars, Paris, Hubert, A-M. & Jaschek, M. eds, Kluwer Academic Publishers, in press
Pottasch S. R. 1984, Planetary Nebulae, Astrophysics and space science library, Eds Reidel Publishing Compagny, Vol. 107, p 87
Stee, Ph., and Araùjo, F.X. 1994, A&A , 292, 221
Stee, Ph., de Araùjo, F.X., Vakili, F., Mourard, D., Bonneau, D., Bosc-Tallon, I., Morand, F., Lawson, P. and Arnold, L., 1995a, A&A, 300, 219
Zickgraf F.-J., Wolf, B., Stahl, O., Humpreys, R.M. 1989, A&A, 220, 206
Zickgraf F.-J. 1990, in Davidson K., Moffat A.F.J., Lamers H.J.G.L.M., eds, IAU Colloquium 113, Kluwer Academic Publishers, Dordrecht. p. 117
Zickgraf F.-J., Stahl, O., Wolf, B. 1992, A&A, 260, 205
Zickgraf F.-J., Humpreys, R.M., Lamers H.J.G.L.M., Smolinski, J., Wolf, B., and Stahl, O. 1996, A&A , 315, 510